

# THEORY OF AN ELECTROSTATIC INSTABILITY DRIVEN BY TRANSVERSE-LONGITUDINAL TEMPERATURE ANISOTROPY IN SPACE CHARGE DOMINATED BEAMS \*

S.M. Lund<sup>a</sup>, D.A. Callahan<sup>a</sup>, A. Friedman<sup>a</sup>, D.P. Grote<sup>a</sup>, I. Haber<sup>b</sup>, and T.F. Wang<sup>c</sup>

<sup>a</sup> Lawrence Livermore National Laboratory, Livermore, CA 94550 USA

<sup>b</sup> Naval Research Laboratory, Washington, DC 20375, USA

<sup>c</sup> Los Alamos National Laboratory, Los Alamos, NM 87545, USA

## Abstract

An unstable electrostatic mode has been observed in particle-in-cell simulations that, for unbunched ion beams with sufficient intensity and thermal anisotropy, transfers thermal energy from the transverse ( $\perp$ ) to the longitudinal ( $\parallel$ ) directions<sup>1-4</sup>. This instability can be important and appears to be insensitive to the details of the initial distribution as well as the nature of the applied focusing. The unstable mode is characterized by an axial wavelength comparable to the beam radius and growth rates comparable to the frequency of  $\perp$  particle betatron oscillations. We present a theory of this instability based on the work of Wang and Smith<sup>5</sup>. This theory employs a continuous focusing model in the limit of strong thermal anisotropy with a warm,  $\perp$  KV distribution and a cold,  $\parallel$  distribution. The predicted mode structure is found to compare favorably with simulations carried out over a range of space-charge strength.

## 1 INTRODUCTION

In a continuous focusing (CF) channel, a thermal equilibrium (TE) beam distribution represents a stable, maximum entropy state that an arbitrary initial distribution will relax to under the influence of collisions<sup>6</sup>. Although collective processes and phase mixing can enhance the rate of relaxation, the beam lifetime in the machine is often insufficient to allow significant relaxation. Moreover, in real accelerators, the focusing is usually periodic, and in this situation there is no known TE distribution. Nevertheless, distributions that more closely resemble a CF TE distribution are expected to have less free energy to drive instabilities. This renders thermodynamic concepts like beam temperature useful for non TE distributions.

Although temperature is, strictly speaking, a thermodynamic quantity, one can define local kinetic temperatures (energy units) by  $T_i/2 = \langle (p_i - \langle p_i \rangle)^2 \rangle / 2m = mv_{th,i}^2/2$ , where  $m$  is the particle mass,  $p_i$  is the  $i = x, y, z$  particle momentum,  $v_{th,i}$  is the  $i$ th local thermal velocity component, and  $\langle \dots \rangle$  denotes an average over the momentum space degrees of freedom in the particle distribution. Here and henceforth, we have adopted a nonrelativistic model for simplicity in presentation. Differences in these kinetic temperatures (or equivalently momentum spreads) provide a measure of deviations from an isotropic TE, and such dif-

ferences can provide free energy for so-called “equipartitioning” instabilities that drive the beam closer to TE<sup>7</sup>.

$\perp$ - $\parallel$  temperature anisotropies tend to naturally develop in accelerators<sup>6,8</sup>. For example, consider an ion diode with particle energy  $\mathcal{E}_b$  ( $\sim 50$  keV typical) and source temperature  $T$  ( $\sim 0.1$  eV typical). In the absence of  $\perp$ - $\parallel$  coupling, one would expect the final axial ( $z$ -direction) temperature to be strongly cooled with  $T_z = T^2/2\mathcal{E}_b$ . On the other hand, one would expect little accelerative change in  $\perp$  temperatures with  $T_x = T_y \sim T$ , consistent with any  $\perp$  beam compression,  $\perp$  instabilities, etc. These effects suggest a strongly anisotropic beam emerging from the diode. Further  $\perp$ - $\parallel$  anisotropy can develop in the transport following the diode. Neglecting  $\perp$ - $\parallel$  coupling,  $T_z\tau \simeq const$ , where  $\tau$  is the beam pulse duration, and  $T_z$  will evolve consistently with any  $\parallel$  beam expansion or compression during acceleration. Some change in  $T_z$  can also be caused by the thermalization of  $\parallel$  space-charge waves launched by acceleration errors. On the other hand, nonlinear forces associated with focusing aberrations and nonuniform space charge (from instabilities, various beam manipulations, etc.), can lead to increased  $\perp$  normalized beam emittance ( $\propto r_b\sqrt{T_x}$ , where  $r_b$  is the beam radius) while only producing small changes in  $T_z$ .

In high intensity applications such as Heavy-Ion Fusion (HIF), the need for a small focal spot radius  $r_s$  leads to interrelated constraints on the beam  $\perp$  emittance, space-charge strength, and  $\parallel$  momentum spread, as well as machine misalignments and aberrations in the final focus optic<sup>9</sup>. For a final magnetic optic, dispersion results in a limit of allowable  $\parallel$  momentum spread that can be estimated as  $\Delta p/p < r_s/8\theta d$ . Here  $p = \langle p_z \rangle$  and  $\Delta p = \sqrt{2\langle (p_z - p)^2 \rangle}$  are the axial momentum and momentum spread,  $d$  is the distance from the final optic to the focal spot, and  $\theta$  is the beam convergence angle to the spot. This typically results in spread limits of less than  $\Delta p/p \sim 1\%$ . If the  $\perp$  and  $\parallel$  beam temperatures must remain similar, this will introduce an additional constraint that must be considered. Moreover, if any bends are present, dispersion can result in further momentum spread limits that  $\perp$ - $\parallel$  equilibration can influence<sup>8</sup>.

In most accelerators, particle collision times are generally much longer than the beam lifetime in the machine. Hence collision induced equipartitioning is usually negligible. On the other hand, rapid kinetic instabilities can result in significant equipartitioning. Thus it is prudent to understand any such instabilities so they can be properly

\* This research was performed under the auspices of the US DOE by LLNL, NRL, and LANL under contracts W-7405-ENG-48, DE-AI02-93ER40799, and DE-AI02-94ER54232.

accounted for in machine design.

In this paper, we present simulation (Sec. 2) and theory (Sec. 3) on an intense-beam collective mode that produces a rapid transfer of thermal energy from the  $\perp$  to the  $\parallel$  degrees of freedom for sufficient  $\perp$ - $\parallel$  thermal anisotropy. The beam is unbunched, and nonlinear space-charge forces associated with the unstable electrostatic mode produce this energy exchange rather than  $\perp$ - $\parallel$  coupling induced by the shape of the beam ends. For simplicity, all analysis is carried out for an axisymmetric ( $\partial/\partial\theta = 0$ ) beam propagating without acceleration in a continuous focusing channel with a linear radial focusing force. This focusing arrangement can represent the average effects of a lattice of alternating gradient electric or magnetic quadrupoles, or a periodic solenoidal magnetic field for a beam with zero total canonical angular momentum<sup>10</sup>.

## 2 PIC SIMULATIONS

Particle-in-cell (PIC) simulations were carried out with the electrostatic WARP code<sup>2,8</sup>. An axisymmetric ( $rz$ ) package of the WARP code suite that neglects self-magnetic field effects was employed with periodic boundary conditions axially, and a grounded, perfectly conducting cylindrical beam pipe transversely. Simulations employed 100 k to 1 M particles, and typical grid dimensions consisted of 32 radial and 256 axial zones. When  $T_z$  was sufficiently cold, Gaussian smoothing was employed in the axial direction to suppress a  $\parallel$  numerical grid instability. The initial  $\perp$  distribution of beam particles had zero canonical angular momentum and was either KV [uniform density and a parabolically decreasing temperature profile in the radial coordinate  $r = \sqrt{x^2 + y^2}$ , see Ref. 6 and Sec. 3] or semi-Gaussian (SG) [uniform density and a uniform temperature Gaussian in  $\perp$  momentum space]. The initial  $\parallel$  distribution had uniform density and Gaussian momentum spread. The instability is seeded from noise associated with the finite particle statistics.

Typical runs employed:  $K^+$  ion at  $\mathcal{E}_b = \langle p_z \rangle^2 / 2m = 10$  MeV axial kinetic energy, equilibrium beam radius  $r_b = 2.5$  cm, beam current  $I = 5$  A, and conducting pipe radius  $r_p \geq 2r_b = 5$  cm. The spatial average  $\perp$  beam temperature  $\hat{T}_x = \hat{T}_y = (2\pi \int_0^{r_b} dr r T_x) / \pi r_b^2$  was then consistently set as follows (in an rms equivalent beam sense<sup>6</sup> for an initial SG distribution). Denote the angular frequency of  $\perp$  particle oscillations in the equilibrium fields in the absence (i.e.,  $I = 0$ ) and presence (specified  $I$ ) of space charge by  $\nu_0$  and  $\nu$ , respectively. Using the equilibrium envelope equation, these so-called ‘‘betatron’’ frequencies can be expressed as<sup>10</sup>

$$\begin{aligned} \nu_0^2 &= 4\hat{T}_x / mr_b^2 + \hat{\omega}_p^2 / 2, \\ \nu^2 &= \nu_0^2 - \hat{\omega}_p^2 / 2 = 4\hat{T}_x / mr_b^2, \end{aligned} \quad (1)$$

where  $\hat{\omega}_p$  is the beam plasma frequency. Then  $\hat{T}_x$  was set to achieve a specified tune depression  $\nu/\nu_0$  satisfying  $0 \leq \nu/\nu_0 \leq 1$ , where  $\nu/\nu_0 \rightarrow 1$  and  $\nu/\nu_0 \rightarrow 0$  correspond to the warm- and cold-beam limits, respectively.

With  $\hat{T}_x$  fixed,  $\nu_0$  (i.e., the external focusing) was then set consistently with Eq. (1). For  $\nu/\nu_0 \sim 0.1$  to 0.4, these parameters are representative of those in the low energy end of linear induction accelerators for Heavy Ion Fusion<sup>9</sup>. The  $\parallel$  temperature  $T_z$  was set as a fraction of  $\hat{T}_x$ . Axial grid lengths were chosen sufficiently short for the  $\parallel$  variations of the unstable mode to be well resolved, but sufficiently long where 5 or more wavelengths of variation were simulated to reduce the influence of the periodic boundary conditions. This resulted in grid lengths of 10 to 25 cm. Timesteps for the particle advance were chosen such that  $dt < 0.01/\nu_0$ .

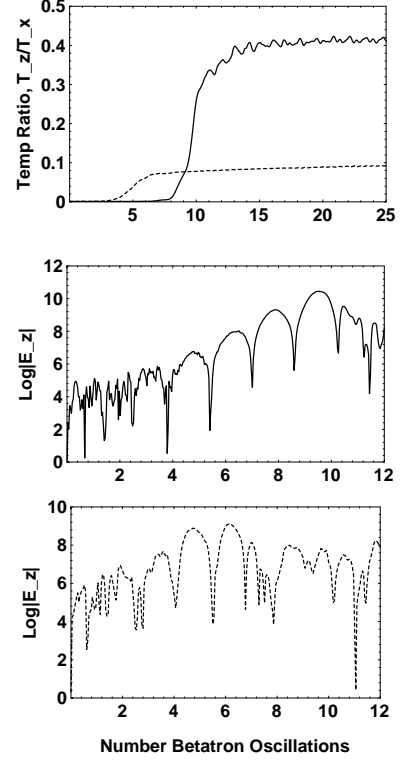


Figure 1: Temperature anisotropy  $T_z/\hat{T}_x$  (top, SG and KV) and the log of the absolute value of the axial electric field  $\ln |E_z|$  (middle for KV, and bottom for SG) versus the number of undepressed betatron oscillations  $\nu_0 t / 2\pi$ .

Results of simulations illustrating properties of a space-charge mode that transfers thermal energy from the  $\perp$  to the  $\parallel$  directions are presented in Figs. 1 and 2. The simulations are for initial  $\nu/\nu_0 = 0.45$ ,  $T_z = 0.01\hat{T}_x$ , a 13.4 cm axial beam length, and  $r_p = 2r_b$ . Results are shown for both initial KV (solid curves) and SG (dashed curves)  $\perp$  distributions. In Fig. 1, the anisotropy ratio  $T_z/\hat{T}_x$  is plotted as a function of the number of undepressed betatron oscillations of an equilibrium particle,  $\nu_0 t / 2\pi$ , where  $t$  is the time. Evidently, in the initial quiescent period the growth in  $T_z/\hat{T}_x$  starts from the noise, followed by a period of exponential growth, and then saturation with  $T_z/\hat{T}_x \sim 0.4[0.1]$  (results given for initial KV with SG values in ‘‘[ ]’’ brackets). This instability leads to increased  $T_z$  and decreased  $\hat{T}_x$  as energy is exchanged. Phase space plots of the mode have been presented elsewhere<sup>3,4</sup>. Also in Fig. 1, the log of the abso-

lute value of the axial electric field,  $\ln |E_z|$ , is plotted (arbitrary units) for a fixed location moving with the equilibrium beam as a function of  $\nu_0 t/2\pi$ . Little variation in structure is observed with the choice of location, suggesting an absolute instability. These plots suggest that a single unstable mode is dominating the evolution with an oscillation period and  $e$ -fold time of approximately 3.2[2.8] and 0.82[1.1] undepressed betatron oscillations, respectively. The radial and axial structure of the perturbed electrostatic potential  $\delta\phi$  describing this mode was extracted with a discrete Fourier transform diagnostic. The dominant axial wavelength  $\lambda$  of  $\delta\phi$  was well expressed with  $\lambda/r_b = 1.3$ [1.1] and the radial mode structure of this harmonic component is shown in Fig. 2 for  $\nu_0 t/2\pi = 9.2$ [3.9]. Note that  $\delta\phi$  is peaked at the center with one radial node within the beam ( $r < r_b = 2.5\text{cm}$ ) and has small amplitude outside the beam ( $r_b < r \leq r_p = 5\text{cm}$ ).

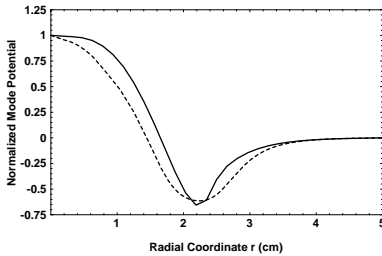


Figure 2: Normalized electrostatic potential of the unstable mode  $\delta\phi/\delta\phi(r=0)$  versus radial coordinate  $r$ .

The simulations indicate that the essential features of this instability are similar for both initial KV and SG  $\perp$  distributions. However, since the SG is not a real equilibrium, the lack of detailed radial force balance influences the initial evolution of the mode, complicating the interpretation of the onset of instability (note the shift in Fig. 1). Moreover, details of the saturation are different for the KV and SG  $\perp$  distributions, with wave breaking in the KV distribution leading to a trapped particle phase-space that may represent an intermediate state on a longer timescale evolution. The KV and SG initializations also have differing numerical collision properties, further complicating interpretations. Preliminary data is presented in Table 1 on the space-charge threshold ( $\nu/\nu_0$  less than indicated values leads to instability) and the saturation level (in  $T_z/\hat{T}_x$ ) of the instability. Data is tabulated for both initial KV and SG  $\perp$  distributions for several values of initial temperature anisotropy ( $T_z/\hat{T}_x$ ). Note that the threshold is a strong function of the initial anisotropy and depends weakly on the type of initial distribution. Saturation occurs when  $T_z$  is a fraction of  $\hat{T}_x$ , with the value depending on the initial anisotropy, space-charge strength, and distribution type. Growth rates of the unstable mode are larger for strong initial anisotropy and space-charge strength. Smaller growth rates can render simulations difficult due to the noise associated with the finite particle statistics.

Finally, previous studies<sup>1,4</sup> suggest that the instability only transfers  $\perp$  thermal energy to the  $\parallel$  direction and

Table 1: Instability threshold and saturation properties.

Initial $T_z/T_x$	Threshold $\nu/\nu_0$	
	KV	SG
0.001	0.69	0.74
0.01	0.76	0.80
0.1	0.48	?

Initial $T_z/T_x$	Saturated $T_z/T_x$ for Initial KV and $\nu/\nu_0 =$				
	0.4	0.5	0.6	0.7	0.8
0.001	0.55	0.18	0.04	—	—
0.01	0.59	0.31	0.07	0.09	—
0.1	0.42	—	—	—	—

Initial $T_z/T_x$	Saturated $T_z/T_x$ for Initial SG and $\nu/\nu_0 =$				
	0.4	0.5	0.6	0.7	0.8
0.001	0.10	0.14	0.19	0.08	—
0.01	0.12	0.10	0.16	0.14	0.11

not vice-versa when  $T_z > \hat{T}_x$ . Full 3D simulations have also been carried out with both alternating gradient and CF channels and the results are similar those presented here.

### 3 THEORY

Neglecting particle correlations and collisions, the beams simulated in Sec. 2 are described in terms of a single-particle distribution function  $f$  that is a function of the coordinate  $\mathbf{x}$ , momentum  $\mathbf{p}$ , and time  $t$ , and evolves according to the Vlasov equation

$$\left\{ \frac{\partial}{\partial t} + \frac{\partial H}{\partial \mathbf{p}} \cdot \frac{\partial}{\partial \mathbf{x}} - \frac{\partial H}{\partial \mathbf{x}} \cdot \frac{\partial}{\partial \mathbf{p}} \right\} f(\mathbf{x}, \mathbf{p}, t) = 0. \quad (2)$$

Here,  $H = \mathbf{p}^2/2m + m\nu_0^2 r^2/2 + q\phi$  is the Hamiltonian,  $q$  is the particle charge, and  $\phi$  satisfies the Poisson equation  $\nabla^2 \phi = 4\pi q \int d^3p f$  subject to the boundary condition  $\phi(r = r_p) = \text{const}$ . To perform a conventional equilibrium/stability analysis, we expand

$$\begin{aligned} \phi &= \phi^0(r) + \delta\phi(r, \omega, k_z) e^{-i(\omega t - k_z z)}, \\ f &= f^0(\mathbf{x}, \mathbf{p}) + \delta f(r, \mathbf{p}, \omega, k_z) e^{-i(\omega t - k_z z)}, \end{aligned} \quad (3)$$

where equilibrium quantities (superscript zero) correspond to  $\partial/\partial t = 0$  solutions to Eq. (2) with  $\delta\phi = 0 = \delta f$  and  $\delta\phi$  and  $\delta f$  are normal mode perturbations with angular frequency  $\omega$  and wavenumber  $k_z = 2\pi/\lambda$ . We assume a  $\perp$  KV and  $\parallel$  Gaussian  $f^0$  defined by<sup>6,10</sup>

$$f^0 = \frac{\hat{n}}{2\pi m} \delta(H_{\perp}^0 - 2\hat{T}_x) \frac{\exp\left[-\frac{(p_z - mv_b)^2}{2mT_z}\right]}{(2\pi mT_z)^{1/2}}. \quad (4)$$

Here,  $v_b = \langle p_z \rangle / m$  is the axial beam velocity,  $\delta(x)$  is the Dirac delta-function, and  $H_{\perp}^0 = \mathbf{p}_{\perp}^2/2m + m\nu_0^2 r^2/2 + q\phi^0$  with  $\mathbf{p}_{\perp} = p_x \hat{x} + p_y \hat{y}$ . The form of  $f^0$  is consistent with undepressed and depressed  $\perp$  particle oscillations with frequencies  $\nu_0$  and  $\nu$  given by Eq. (1) with  $\hat{\omega}_p^2 = 4\pi q^2 \hat{n}/m$  and beam edge radius  $r_b$ . For  $0 \leq r < r_b$ , Eq. (4) also corresponds to uniform density,  $\int d^3p f^0 = \hat{n} = \text{const}$ , and a parabolic  $\perp$  temperature profile,  $\int d^3p (\mathbf{p}_{\perp}^2/2m) f^0 = 2\hat{n}\hat{T}_x(1 - r^2/r_b^2)$ .

The linear eigenvalue equation for the perturbed potential  $\delta\phi$  can be derived by linearizing the Vlasov equation (2) and inverting the resulting equation for  $\delta f$  with the method of characteristics and inserting the result in Poisson's equation. After some algebraic manipulation, this results in

$$\left\{ \frac{1}{r} \frac{\partial}{\partial r} r \frac{\partial}{\partial r} - k_z^2 \right\} \delta\phi = \frac{\hat{\omega}_p^2 r_b}{4\hat{T}_x/m} \delta(r-r_b) [\delta\phi + \kappa_1] \Big|_{p_\perp=0} + \hat{\omega}_p^2 \Theta(r_b-r) \left[ \frac{m^2}{p_\perp} \frac{\partial}{\partial p_\perp} \kappa_1 + i k_z^2 \kappa_2 \right] \Big|_{p_\perp^2/2m=T_x}, \quad (5)$$

where  $\Theta(x)$  is the Heaviside step-function, and  $\kappa_1$  and  $\kappa_2$  are equilibrium orbit integrals defined by

$$\begin{aligned} \kappa_1 &= i \int \frac{d\psi}{2\pi} \int_{-\infty}^0 d\tau \left( \Omega - i \frac{k_z^2 T_z}{m} \tau \right) \\ &\times \delta\phi[\tilde{r}(\tau)] \exp \left[ -\frac{k_z^2 T_z}{2m} \tau^2 - i\Omega\tau \right], \quad (6) \\ \kappa_2 &= i \int \frac{d\psi}{2\pi} \int_{-\infty}^0 d\tau \tau \delta\phi[\tilde{r}(\tau)] \exp \left[ -\frac{k_z^2 T_z}{2m} \tau^2 - i\Omega\tau \right]. \end{aligned}$$

Here,  $T_x \equiv 2\hat{T}_x(1-r^2/r_b^2)$ ,  $\Omega \equiv \omega - k_z v_b$ , and the equilibrium characteristics are defined by  $\tilde{r}^2(\tau) \equiv r^2 \cos^2(\nu\tau) + (rp_\perp/m\nu) \cos(\ ) \sin(2\nu\tau) + (p_\perp/m\nu)^2 \sin^2(\nu\tau)$ .

Equation (5) is a difficult integro-differential equation that must be solved for  $\Omega$  and  $\delta\phi$  simultaneously. Wang and Smith<sup>5</sup> derived the dispersion relation corresponding to Eq. (5) in the limit of infinite thermal anisotropy ( $T_z/\hat{T}_x \rightarrow 0$  by coupling together earlier transverse solutions ( $T_z = 0$  and  $k_z = 0$ ) by Gluckstern<sup>11</sup> for  $k_z \neq 0$ . In this procedure  $\delta\phi$  is expanded within the beam ( $0 \leq r \leq r_b$ ) as

$$\delta\phi(r) = \delta\phi(r=r_b) + \sum_{n=1}^{\infty} A_n \delta\phi_n(r), \quad (7)$$

where  $\delta\phi_n(r) = (1/2)[P_{n-1}(1-2r^2/r_b^2) + P_n(1-2r^2/r_b^2)]$  is an  $n$ th order  $\perp$  Gluckstern eigenfunction,  $P_n(x)$  is a  $n$ th order Legendre Polynomial, and  $\delta\phi(r=r_b)$  is the potential at the beam edge (generally nonzero). The expansion coefficients  $A_n$  generally depend on  $k_z$  and  $\Omega$  and satisfy recursion relations, which together with an interface ( $r=r_b$ ) jump condition on  $\delta\phi$ , yields a dispersion relation expressible in terms of an infinite determinant.

Approximate numerical solutions to this dispersion relation can be found by truncating the series [ $n < n_{max}$  in Eq. (7)] to obtain a finite determinant dispersion relation<sup>5</sup>. Solutions for  $\Omega/\nu_0 = (\omega - k_z r_b)/\nu_0$  are parameterized by  $\nu/\nu_0$ ,  $k_z r_b$ , and  $r_b/r_p$ . The number of distinct mode branches found is  $n_{max}(n_{max} + 2)$  or  $(n_{max} + 1)^2$  for  $n_{max}$  even or odd. The branches are characterized according to their limiting properties. For  $k_z r_b \rightarrow 0$ ,  $n_{max}(n_{max} + 1)$  branches corresponding to  $n$ th order  $\perp$  Gluckstern modes<sup>11</sup> are found (labeled  $T_n$ ) with  $\delta\phi \propto \delta\phi_n$  for  $r \leq r_b$  and  $\delta\phi = 0$  for  $r \geq r_b$ . Properties of this  $\perp$  limit dispersion relation have been described

elsewhere<sup>10,11</sup>. For long wavelength perturbations with  $k_z r_b \ll 1$  and  $\hat{T}_x \rightarrow 0$  ( $\nu \rightarrow 0$ ), a single branch (labeled  $L_1$ ) corresponding to an ‘‘ordinary’’ cold-beam  $\parallel$  mode is found. This limiting form mode has  $\delta\phi \propto I_0(k_z r)$  for  $r \leq r_b$  with  $I_0(x)$  a 0th order modified Bessel Function and  $\Omega^2 = (\hat{\omega}_p^2/2)(k_z r_b)^2 \ln(r_p/r_b)$ . Other branches (labeled  $L_n$  with  $n = 2, 4, \dots, n_{max} - 1$  or  $n_{max}$ ) are found to reduce for long wavelengths ( $k_z r_b \ll 1$ ) and weak space-charge ( $\nu \rightarrow \nu_0$ ) to reduce to a little known class of  $\perp$  coupled  $\parallel$  modes. These modes have  $\delta\phi \propto \delta\phi_n$  within the beam and

$$\Omega^2 = \frac{\hat{\omega}_p^2}{8n(n+1)} (k_z r_b)^2 \int_0^{2\pi} \frac{dx}{2\pi} P_n(\cos x).$$

In general, a large  $n_{max}$  truncation will result a high-order polynomial dispersion relation with many branches; some of which describe low-order modes and others, high-order modes. One takes  $n_{max}$  sufficiently large to accurately represent modes of interest, but small enough to reduce the number of branches and facilitate mode identification. Instabilities arise in parameter regimes where two or more branches of  $\Omega$  ‘‘collide’’ and coalesce. Unfortunately, many of these instabilities, particularly higher-order ones, are associated with unphysical features of the KV model<sup>10</sup>. Nevertheless, we believe that a low-order confluent branch where the  $T_2$  and  $L_2$  branches coalesce describes the instabilities observed in Sec. 2. This low-order  $T_2$ - $L_2$  confluent branch may also represent a non-pathological KV instability that persists for more realistic (non-singular) equilibrium distribution functions.

Comparisons between the confluent  $T_2$ - $L_2$  mode branch and simulations are presented in Figs. 3 and 4. All simulations were seeded from noise and it is assumed that a single unstable mode dominates the evolution. In the theory, an  $n_{max} = 4$  truncation was employed. In Fig. 3, the radial eigenfunction  $\delta\phi$  of the  $T_2$ - $L_2$  mode ( $k_z$  selected for maximum growth rate) is compared with simulation and  $\perp$  ( $k_z \rightarrow 0$ ) theory for  $\nu/\nu_0 = 0.45$  and  $r_p/r_b = 2$ . Note that the  $T_2$ - $L_2$  has similar structure to the  $\perp T_2$  mode, but has finite amplitude at the beam edge ( $r=r_b$ ) and is unstable, in contrast to the  $\perp$  mode. Also in contrast to the  $\perp T_2$  mode, where  $\delta\phi_2$  is independent of  $\omega$ , the radial structure of  $\delta\phi$  varies with  $\Omega$  and  $k_z$  for the  $T_2$ - $L_2$  mode. In Fig. 4 the normalized axial wavenumber, oscillation frequency, and growth rate of the  $T_2$ - $L_2$  mode is compared to the simulation results over the range of space-charge strength  $0.3 \leq \nu/\nu_0 \leq 0.5$ . The theory curves were generated employing the wavenumber  $k_z r_b$  with maximum  $\text{Im } \Omega/\nu_0$  growth rate at specified  $\nu/\nu_0$ . The spreads about the simulation points indicate measurement uncertainties. For  $\nu/\nu_0 \geq 0.4$  the theory agrees reasonably well with the simulations outside of a slightly lower simulated growth rate that is likely due to the finite axial temperature employed in the simulations (initial  $T_z < 0.01\hat{T}_x$ ). For  $\nu/\nu_0 < 0.4$ , low-order KV instabilities of the  $T_2$ ,  $T_3$ , and  $T_4 \perp$  Gluckstern modes<sup>10</sup> may produce the systematic deviations observed from the results predicted by the  $T_2$ - $L_2$

branch. Extension into this strong space-charge regime will likely require systematic mode seeding to avoid exciting such unphysical  $\perp$  KV instabilities. Approximate expressions for the mode density, temperature, and flow velocity perturbations have been derived from a fluid theory<sup>10</sup> (using the kinetic theory dispersion relation) for use in future mode seeding studies.

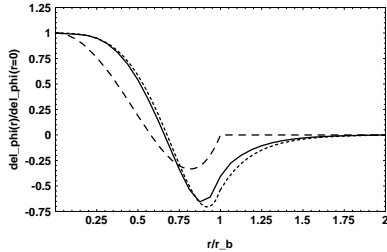


Figure 3: Eigenfunction comparisons for simulation (solid), 3D  $T_2$ - $L_2$  confluent mode theory (dotted), and  $\perp$   $T_2$  mode theory (dashed).

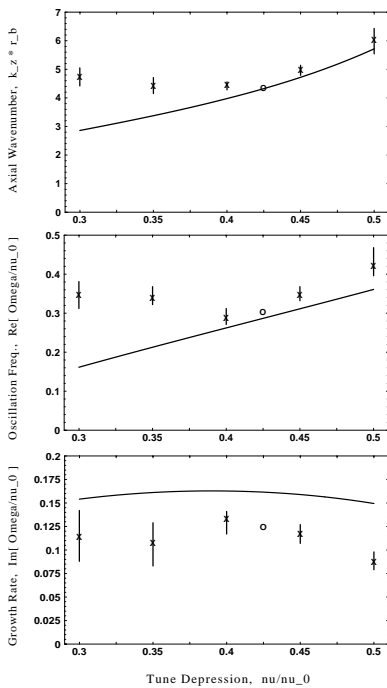


Figure 4: Normalized mode axial wavenumber ( $k_z r_b$ ), oscillation frequency ( $\text{Re } \Omega/\nu_0$ ), and growth rate ( $\text{Im } \Omega/\nu_0$ ) versus tune depression ( $\nu/\nu_0$ ) from theory and simulation.

## 4 CONCLUSIONS

Simulation and theory have been presented characterizing an electrostatic instability that can transfer thermal energy from the  $\perp$  to the  $\parallel$  directions for an intense, unbunched beam with sufficient thermal anisotropy ( $T_z/\hat{T}_x < 1$ ). General features of this instability are insensitive to the specific form of the applied focusing and initial distribution, and therefore, a  $\perp$  KV model was used to explore the idealized mode structure. The instability has short axial wavelength ( $\lambda \sim r_b$ ) with growth rates and oscillation frequencies comparable to the depressed betatron fre-

quency ( $\text{Re } \Omega \sim \text{Im } \Omega \sim \nu$ ). The unstable mode has an anisotropy (initial value of  $T_z/\hat{T}_x$ ) dependent threshold in space-charge strength ( $\nu/\nu_0$ ) and saturates when the  $\parallel$  temperature ( $T_z$ ) is a fraction of the  $\perp$  temperature ( $\hat{T}_x$ ). Since  $\parallel$  accelerative cooling and  $\perp$  emittance increases can contribute to the anisotropy that drives the instability, the mode needs to be better understood to assess impact on machine design. The energy exchange associated with the instability leads to decreased  $\perp$  emittance with increased  $\parallel$  momentum spread. Whether this effect is beneficial or harmful will depend on the details of a particular application. Possible consequences of the instability can be estimated by assuming that  $T_z$  remains saturated during transport at a set fraction of  $\hat{T}_x$  if significant  $\perp$ - $\parallel$  anisotropy would have developed in the absence of the unstable mode. Equipartitioned design concepts have also been applied to bunched beams in rf linacs<sup>12</sup>, where the  $\perp$  and  $\parallel$  focusing can be adjusted to maintain equilibration. Proper modeling this instability also has implications for simulations, since it requires the resolution of short axial wavelengths in simulations of long, “unbunched” beams.

## ACKNOWLEDGMENTS

The authors wish to acknowledge useful conversations with J.J. Barnard, R.C. Davidson, and E.P. Lee.

## 5 REFERENCES

- [1] A. Friedman, D.A. Callahan, D.P. Grote, A.B. Langdon, and I. Haber, “Studies of Equilibration Processes in Heavy-Ion Fusion Beams,” *Bull. Am. Phys. Soc.* **35**(9), 2121 (1990).
- [2] D.A. Callahan, “Simulations of Longitudinal Beam Dynamics of Space-Charge Dominated Beams for Heavy Ion Fusion,” Ph.D. Thesis, University of California, Davis, 1994.
- [3] I. Haber, D.A. Callahan, A. Friedman, D.P. Grote, and A.B. Langdon, *J. Fusion Eng. Design* **32**, 159 (1996).
- [4] I. Haber, D.A. Callahan, A. Friedman, D.P. Grote, S.M. Lund, and T.-F. Wang, “Characteristics of an Electrostatic Instability Driven by Transverse-Longitudinal Temperature Anisotropy,” *Nuc. Inst. Meth.*, in press (1998).
- [5] T.F. Wang and L. Smith, *Part. Accel.* **12**, 247 (1996).
- [6] M. Reiser, *Theory and Design of Charged Particle Beams* (John Wiley, New York, 1994), and references therein.
- [7] I. Hofmann, *Phys. Rev. E* **57**, 4713 (1998).
- [8] S.M. Lund, J.J. Barnard, G.D. Craig, A. Friedman, D.P. Grote, H.S. Hopkins, T.C. Sangster, W.M. Sharp, S. Eylon, T.J. Fessenden, E. Henestroza, S. Yu, and I. Haber, “Numerical Simulation of Intense-Beam Experiments at LLNL and LBNL,” *Nuc. Inst. Meth.*, in press (1998).
- [9] E.P. Lee, in *Heavy Ion Inertial Fusion*, M. Reiser, T. Godlove, and R. Bangerter, Eds. (American Institute of Physics, New York, NY, 1986; AIP Conference Proceedings **152**), p. 461.
- [10] S.M. Lund and R.C. Davidson, “Warm-Fluid Description of Intense Beam Equilibrium and Electrostatic Stability Properties,” *Phys. Plasmas*, in press (1998).
- [11] R.L. Gluckstern, in *Proceedings of the 1970 Proton Linear Accelerator Conference*, Batavia, IL, edited by M.R. Tracy (National Accelerator Laboratory, Batavia, IL, 1971), p. 811.
- [12] M. Reiser and N. Brown, *Phys. Rev. Lett.* **74**, 1111 (1995).